

Static and Dynamic Combined Effects on the Thermal Conductivity of Water Based Ironoxide Nanofluids: Experiments and Theories

A. Arifutzzaman^{*1,4}, A. F. Ismail², M. Z. Alam³, A. A. Khan⁴, Navid Aslfattahi⁵, R. Saidur^{1,6}

¹Research Centre for Nanomaterials and Energy Technology (RCNMET), School of Science and Technology, Sunway University, No. 5, Jalan Universiti, Bandar Sunway, Petaling Jaya, 47500 Selangor Darul Ehsan, Malaysia.

²Department of Mechanical Engineering, Faculty of Engineering, International Islamic University Malaysia, Malaysia

³Department of Biotechnology Engineering, Faculty of Engineering, International Islamic University Malaysia, Malaysia

⁴Department of Manufacturing and Materials Engineering, Faculty of Engineering, International Islamic University Malaysia.

⁵Department of Mechanical Engineering, Faculty of Engineering, University of Malaya, 50603, Kuala Lumpur

⁶Department of Engineering, Lancaster University, Lancaster, LA1 4YW, UK

*Corresponding Author E-mail: arifrahat@sunway.edu.my

Abstract

Reasoning of particular mechanism of anomalous thermal transport behaviors are not identified yet for the nanofluids. In this research, thermal conductivity of maghemite (MH) nanoparticles dispersed deionized water (DW) nanofluids (MH/DW) have been evaluated for the first time using the modified effective medium theories (EMTs). EMTs have been modified with the consideration of static and dynamic effects combinedly for the analysis of anomalous behaviors of thermal conductivity enhancements of the spherical nanoparticles dispersed nanofluids. MH nanoparticles (~ 20 nm) were synthase using chemical co-precipitation techniques. MH/DW nanofluids were prepared with the varying MH nanoparticles loading in DW and thermal conductivity was measured using KD2 pro device. The thermal conductivity enhancement (~ 32 %) were found to be increased linearly with the increasing MH nanoparticle concentration and nonlinearly with the increasing temperature. Existing Maxwell and Maxwell Gantt EMA (MG-EMA) models exhibited awful under-prediction from experimental thermal conductivities of MH/DW nanofluids. Modified model with considering static and dynamic mechanisms of MH nanoparticles combinedly showed reasonably very good agreement with the experimental thermal conductivities of MH/DW nanofluids at elevated temperature. This modified model opens the new windows to analyze the insight of the thermophysical properties of various types of nanofluids by introducing potential parameters.

Keywords: Nanofluids, Thermal conductivity, Maghemite, Effective-Medium-Theories, Combined effects.

Introduction

Nanofluid is the new type of engineering material comprising of nanometer-sized (1-100 nm) solid nanoparticles in the base fluids [1]. It offers useful applications in industrial fluids system as coolant [2] and lubricant fluids [3]. With the comparison of modern nanotechnology and

orthodox thermal science, nanofluids are now offering significant potential [4] in heat transfer area as enhanced thermal transport media [5]. Different chemical and physical aspects have been anticipated to play their particular vibrant roles in the heat transfer performances of nanofluids such as volume fraction [6], size, shape [7] and the species of nanoparticles along with the temperature, pH value of the fluids, Brownian motion and aggregation of nanoparticles [1, 8]. For the fundamental study, analysis of the thermal conductivity property of the magnetic nanofluids is very significant. Likewise, to produce applied thermal devices using magnetic nanofluid such as, cooling loops, new type of heat exchangers and energy alteration systems where very effective thermal conductive behaviors are significantly desirable [2]. Nanofluids can widely be implicated to the miniaturized modern technology in many engineering applications such as, transportation, machining operations, electronics cooling, military systems as well as Heating Ventilations and Air-Conditioning (HVAC) systems [9]. Iron oxide is the commonly used metal oxide nanoparticles in the nanofluids. Among the various iron oxides, magnetite and maghemite have collected a widespread attention because of their unique combination of super-magnetic behaviours and high magnetization to the viable implication in various sectors, despite the fact that they have lower saturation magnetization and specific power loss, non-toxic and stable against oxidation than metallic particles [2, 10]. Chemical coprecipitation technique is one of the simplest chemical pathway and solution-based method for synthesis of ironoxide nanostructures [8, 11].

Even though the particular mechanism of thermal transport behavior has not identified yet for the nanofluids. However, various theoretical explanations to explain the mechanism reasoning the anomalous behaviour of the thermal properties such as thermal conductivity of nanofluids. Those are found to be considered Brownian motion of particles [12], micro convection of cells [13], liquid layering, ballistic transport of energy carriers, and nanoparticle percolation inside the base fluids [14]. Thermal conduction mechanism of spherical nanoparticles containing nanofluids is related to Brownian motion and aggregation or clustering of nanoparticles [15]. The presence of a well-organized interfacial liquid molecular layer on the dispersed spherical shaped particles appears to be not only accountable for the anomalous growth of thermal conductivity. This liquid laying mechanism only can work if the size of the particle very tinny such as even less than 10 nm [9]. Water-based magnetic nanoparticles dispersed nanofluids are a distinct class of polar magnetic nanofluids [16]. Many studies have been carried out on the ironoxide particle dispersed nanofluids [17-21]. Magnetic properties are the concentrated studies in ironoxide based magnetic nanofluid area [20, 22]; however very limited number researches have been conducted on thermal conductivity of this

nanofluid. A few reports in the literature related with the measurement of thermal conductivity of ironoxide nanofluids [8, 23]. Temperature dependent thermal conductivities of water-based ironoxide nanofluids are not usually examined as well. Attempt has been taken to develop a combined model considering the dynamic contribution of nanoparticles attached with the Maxwell's model without considering the effect of the interfacial layer in their thermal conductivity model for nanofluids by Prasher, et al., (2005) [24].

A handful of theoretical works have been conducted emphasizing the static and dynamic contributions of nanoparticles combinedly [25-29]. There have been very minimal agreements among all the static and dynamic models developed with the consideration of conduction-based mechanisms and no extensively believed model is still offered to estimate the magnitude and inclinations of the experimentally obtained data on thermal conductivity of iron oxide based nanofluids. To our knowledge no work has been reported on the modification of models with the consideration of combined static and dynamic effects and its implementation to the magnetic maghemite nanoparticle dispersed nanofluids for the analysis of anomalous behaviours of thermal conductivity enhancements with the vitiation of increasing temperature of nanofluids and volume fraction of the particles. In this research work, EMTs have modified with the effect of static and dynamic contribution of the spherical shape of nanoparticles and implemented for the first time to analyze the anomalous behaviors of the MH/DW nanofluids. It was found a very good agreement with the experimentally measured thermal conductivities. This is another outstanding finding in relation to the thermal conductivity enhancements. New correlations for the thermal conductivity as a function of nanofluids temperature and dispersed particles concentration are developed using experimentally acquired data.

Nomenclature			
FESEM	Field Emission Scanning Electron Microscopy	ml	Mili-litter
DW	Deionized water	K_{nf}	Coefficient of thermal conductivity
KB	Boltzmann's constant	K_{dy}	Dynamic thermal conductivity
EMA	Effective Medium Approximation	K_f	Thermal conductivity of base fluids
MG-EMA	Maxwell Gantt Effective Medium Approximation	K_{eff}	Suspension Effective Thermal Conductivity
RPM	Revolution per Minute	K_p	Thermal Conductivity of the solid particles
FWHM	Full width at half maximum	K_{st}	Static Thermal Conductivity
IUM	International Islamic University Malaysia	T	Temperature
VSM	Vibrating Sample Magnetometer	m	Meter

Subscripts		K	kelvin
cp	Complex nanoparticles	μm	Micrometer
c_p	Specific heat	$^{\circ}\text{C}$	Degree Celsius
d	Average article diameter	Greek symbols	
d_s	Inter-particle separation distance	φ	Volume fraction of filler in base fluid
h	Thickness of liquid layer	ρ_{filler}	Density of filler material dispersed
H	Applied Field	ρ_{bf}	Density of base fluid
m_p	Mass contained of the filler	2θ	Bragg's angle

Materials and Methods

Synthesis of Ironoxide ($\gamma\text{-Fe}_2\text{O}_3$) Nanoparticles

20 ml solutions of 0.25 M, Iron (II) sulphate heptahydrate ($\text{FeSO}_4 \cdot 7\text{H}_2\text{O}$) (278.02 g/mol) and 0.5 M, iron (III) nitrate nonahydrate ($\text{Fe}(\text{NO}_3)_3 \cdot 9\text{H}_2\text{O}$), (404.00 g/mol) were prepared separately. All materials were purchased from Fisher Scientific (M) Sdn. Bhd and used as collected. Prepared solutions were mixed using magnetic stirrer with 150 rpm. After 5 minutes, 100 ml solution of 2M, NaOH (40.00 g/mol) was added as precipitating agent dropwise very slowly using a pipette. After addition mixture was continued with the stirring for 30 minutes. The initial brown precipitate turned into black precipitate as magnetite (Fe_3O_4). The precipitate allowed to settle normally for 10 to 15 minutes. The consisting precipitate magnetite particles was isolated by centrifugation (Eppendorf Centrifuge 5804) with 6000 rpm for 5 minutes. Then supernatant clear liquid was decanted from the mixture. Distilled water was added with the isolated precipitate magnetite particles and stirred with 200 rpm for 10 minutes to conduct the repeated washing. Washing process was carried out very carefully for three times in order to remove the small quantities of micron-sized particles of salts such as nitrates and sulphates that might be present in the precipitate. Nitric acid was added to the precipitate and stirred with 400 rpm for 30 minutes to get the pH of 2.5. After that, obtained precipitate was isolated again by centrifugation (6000 rpm, 5 minutes) to decant the supernatant. Then magnetite particles obtained were oxidized to maghemite ($\gamma\text{-Fe}_2\text{O}_3$) through boiling for 30 minutes by 8ml solution of 0.34M $\text{Fe}(\text{NO}_3)_3 \cdot 9\text{H}_2\text{O}$. Subsequently, the precipitate was isolated and washed again by centrifugation (6000 rpm, 5 minutes) repeatedly for three times. The pH of the resulting suspension was about 2. Final product was dried in vacuum oven (VOS 450SD) at room temperature for 12 h.

Structural and Particle Characterization

X-ray Diffractogram (XRD): XRD pattern was recorded on powder samples of synthesized ironoxide particles using a Bruker AXS x-ray diffractometer (Model: Advance, D8) in 2θ range

of 10-90° with a step size of 0.025 degree/step. Characteristic peaks position was analysed for the identification of maghemite ($\gamma\text{-Fe}_2\text{O}_3$) nanoparticles using the JCPDS database. Crystallite size of the particles were determined by the Scherrer's formula ($D = K\lambda/B \cos \theta$). Where, D is the average crystallite size, B is the full width at half maximum (FWHM) of the main peak stated in radians, λ is the wavelength of X-rays ($\lambda=0.154$ nm), θ is the Bragg angle (half of 2θ), K is the Scherrer constant related to crystallite shape which is 0.94 for maghemite.

FESEM Analysis: The morphology of the synthesized maghemite nanoparticles were captured using field emission scanning electron microscopy (FESEM) (Model JEOL JSM-6700F). A few drops of samples were dropped onto the copper stubs and dried using air flow. Then a gold coating was created on the sample with the aid of sputter coating technique. Collected images were analyzed using an image analysis software (OLYMPUS Stream, version 1.9).

Thermogravimetric (TG) Analysis: TG analysis was conducted on as prepared maghemite samples using the module STA7300, Netzsch, Germany. The sample was put on an aluminum crucible with a heating rate of 10 °C/min, within the temperature ranges 25 to 600 °C.

Magnetic Measurements: Magnetic characterization of the powder sample of synthesised ironoxide nanoparticles was conducted by measuring the hysteresis loops at 300K using Lake Shore's vibrating sample magnetometer (VSM) (model no. 7404) with the applied magnetic field within the range of -10kG to 10KG. The saturation magnetization or maximum magnetization (M_{\max}) also estimated for the measured sample.

Preparation of Water based Maghemite Nanofluids

For the illustration of results, Maghemite ($\gamma\text{-Fe}_2\text{O}_3$) is abbreviated as 'MH' and deionized water is expressed as 'DW'. MH nanoparticles dispersed DW nanofluids is expressed as MH/DW. Five different samples were prepared with the increasing MH nanoparticles concentrations in DW base fluid. Prepared MH/DW nanofluid samples concentrations were varied from 0.065 to 0.157 mg/ml and expressed as S1 to S5-MH/DW correspondingly. Volumetric fractions of the nanofluids were estimated by the correlation in Equation 1 [30].

$$\phi_{\text{Filler}} = \frac{\left[\frac{W_{\text{Filler}}}{\rho_{\text{Filler}}} \right]}{\left[\frac{W_{\text{Filler}}}{\rho_{\text{Filler}}} \right] + \left[\frac{W_{\text{DW}}}{\rho_{\text{DW}}} \right]} \times 100\% \quad (1)$$

Where, W_{Filler} is the mass of filler, ρ_{Filler} is the density of filler material dispersed, ρ_{DW} is the water density (998.5 kg/m³) [31] and ϕ_{Filler} is the percentage Volumatic fraction of the filler in DW.

Measurement of Thermal Conductivity

Prepared MH/DW nanofluids thermal conductivity was measured by the KD2 Pro device (Decagon, USA, version 5) using KS-1 single-probe sensor. An up-to-date programmable refrigerated water bath (Model AD07R-40-12E, Polyscience, USA) was used for governing the temperature which can preserve temperature uniformity within ± 0.01 °C. Sensor performance was measured with manufacturer recommended fluid glycerol. About 45 ml of sample was taken into a close vial. A thermocouple was placed inside the vial to monitor the inside sample temperature. Sensor probe was wholly inserted vertically into the sample vial. A schematic illustration of the thermal conductivity measurements is shown in the Figure 1. Considered deviation of the noted temperature was ± 0.5 °C. All measurements were conducted within the same range of temperature 25 to 60 °C. Data was noted for every temperature only after reaching the equilibrium state. For the accuracy purpose, every data was taken repeatedly minimum of 10 times (up to 25 times). Absolute errors of all measurements were found ± 0.001 . Almost 20 % of collected data were not taken for analysis pretending them as outliers. Average values were taken for the analysis. After the above stated cautious measures in procedures and data collection, it gains strong confidence on the experimental results.

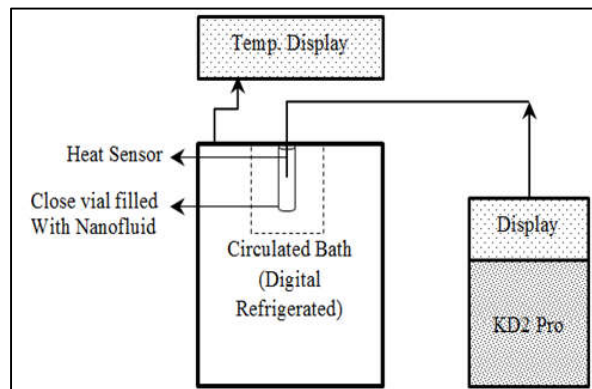


Figure 1: Schematic illustration of thermal conductivity measurement instrument.

Modification of Combined Model for MH Particles

Analytical model introduced by Maxwell [32] is considered as the representative of conventional models as in Equation 7. Where nanofluid's effective thermal conductivity is

dependent only on the thermal conductivity of the dispersed particles and base fluid and particle's volume fraction in the fluid.

$$K_{eff} = \frac{(K_p + 2K_f) + 2\phi(K_p - K_f)}{(K_p + 2K_f) - \phi(K_p - K_f)} \times K_f \quad (7)$$

Where, K_{eff} is the effective thermal conductivity of the nanofluid, K_p is the thermal conductivity of the solid particles dispersed, K_f is the thermal conductivity of the base fluid, and ϕ is the filler volume fraction.

Hasselman and Johnson (1987) [33] adapted and modified the Maxwell's model with introducing Kapitza resistance (interfacial thermal resistance) between the particle and liquid interface as in Equation 8 [9]. Commonly it is recognized as Maxwell Gantt type EMA (MG-EMA) theories and expressed as MG-EMA: HJ model.

$$K_{eff} = \frac{K_p(1-2\alpha) + 2K_f + 2\phi[K_p(1-\alpha) - K_f]}{K_p(1-2\alpha) + 2K_f - \phi[K_p(1-\alpha) - K_f]} \times K_f \quad (8)$$

Where, $\alpha = 2R_{bd} K_f / d$, d is the mean particle diameter, R_{bd} is the interfacial thermal resistance (Kapitza resistance), K_p and K_f are the thermal conductivity of dispersed particles and base fluid correspondingly.

Nanofluid's effective thermal conductivity (K_{eff}) would be the summation of static thermal conductivity (K_{st}) and dynamic thermal conductivity (K_{dy}) ($K_{eff} = K_{st} + K_{dy}$). This combined model is named as 'present model' [25]. Figure 7 illustrates the concept of Brownian motion-based dynamic mechanisms of spherical nanoparticles in the base fluid.

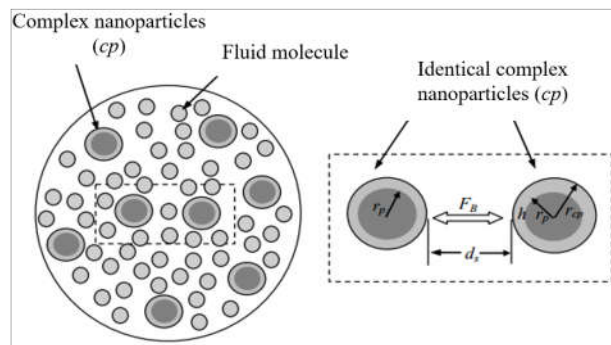


Figure 2: Schematic illustrations of Brownian motion mechanism of spherical particles in the base fluid.

A static thermal conductivity model of the nanofluids considering no-interactions among the particles was developed earlier. Three components from the fluids mixture were considered, particle radius (r_p), thickness ($h=r_{cp}-r_p$) of the interfacial layer among the particle-

fluid medium and the fluid medium. The static thermal conductivity (K_{st}) is expressed as Equation 9 [25, 34].

$$K_{st} = \frac{\varphi\omega(K_p - \omega K_f)[2\gamma_1^3 - \gamma^3 + 1] + (K_p + 2\omega K_f)\gamma_1^3[\varphi\gamma^3(\omega - 1) + 1]}{\gamma_1^3(K_p + 2\omega K_f) - (K_p - \omega K_f)\varphi[\gamma_1^3 + \gamma^3 - 1]} \times K_f \quad (9)$$

In Equation (9), $\gamma = r_{cp}/r_p = 1 + h/r_p$, r_{cp} is the radius of nanoparticle with the interfacial layer (complex nanoparticle), K_{lr} is the thermal conductivity of the interfacial layer and ω (K_{lr}/K_f) is the thermal conductivity ratio of interfacial layer and base liquid [9, 34]

On the other hand, Murshed et al., (2009) [25], (Murshed et al., 2011) [26] deduced a modified Brownian motion term as diffusion coefficient (U_{MBM}) expressed as, $U_{MBM} = \sqrt{2K_B T(1 - 1.5\varphi)/m}$. Where, K_B is the Boltzmann's constant, m is the mass of the particle and T is the fluid temperature. The gross axial heat flux (q_{dy}) because of the motion of nanoparticles causing from the Brownian force (F_B) influencing on them, it was expressed as, $q_{dy}'' \approx -(1/2)nm_{cp}c_{p-cp}d_sU_{MBM}\nabla T$ [25, 35]. Where, n is the number density, m_{cp} , d_s and c_{p-cp} are the mass, average separation distance of complex nanoparticles and specific heat correspondingly. By means of, $nm_{cp} = \rho_{cp}$ in equation with axial heat flux, nanofluids dynamic part of thermal conductivity because of the influence of particles Brownian motion (K_{dy}) is written as, $K_{dy} = (1/2)\rho_{cp}c_{p-cp}d_sU_{MBM}$ [26].

Using, U_{MBM} for complex nanoparticles into K_{dy} and with the use of $\varphi_{cp} = \varphi\gamma^3$, the following ultimate form of Brownian motion contributed thermal conductivity is acquired as Equation 10 [26].

$$K_{dy} = \frac{1}{2}\rho_{cp}c_{p-cp}d_s\sqrt{3K_B T(1 - 1.5\gamma^3\varphi)/2\pi\rho_{cp}\gamma^3r_p^3} \quad (10)$$

Where, $d_s = 0.893 r_{cp}\varphi_{cp}^{-1/3} = 0.893 r_p\varphi^{-1/3}$ [36]. Specific heat (c_{p-cp}) and density (ρ_{cp}) of complex particles could be attained from the designs provided in Murshed et al., (2009) [25]. For $\varphi < 0.002$, the interparticle separation distance, d_s is too big to take place any collusion (interaction) via F_B of particles [25, 37]. For this reason, the dynamic influence of the thermal conductivity, K_{dy} is not so suitable to apply for $\varphi < 0.002$. As mentioned earlier, the effects of both the static and dynamic mechanisms are considered to be additive and the ultimate model in the nanofluids effective thermal conductivity (K_{eff}) can be obtained in Equation 11 by merging the static part from Equation 9 and the dynamic part from Equation 10.

$$K_{eff} = \left\{ \frac{\varphi\omega(K_p - \omega K_f)[2\gamma_1^3 - \gamma^3 + 1] + (K_p + 2\omega K_f)\gamma_1^3[\varphi\gamma^3(\omega - 1) + 1]}{\gamma_1^3(K_p + 2\omega K_f) - (K_p - \omega K_f)\varphi[\gamma_1^3 + \gamma^3 - 1]} \times K_f \right\} + \left\{ \frac{1}{2}\rho_{cp}c_{p-cp}d_s\sqrt{\frac{3K_B T(1 - 1.5\gamma^3\varphi)}{2\pi\rho_{cp}\gamma^3r_p^3}} \right\} \quad (11)$$

However, if there is no layer considered to be existed then, $h=0$, γ and ω fall to 1(one). Then thermal conductivity of the static part in Equation 9 will fall to the Maxwell model as Equation 7 [9, 26].

For the spherical nanoparticle suspended nanofluids, in the assumption of no inter facial layer between the particle and the base fluid, the complex nanoparticles density (ρ_{cp}) and its specific heat (c_{p-cp}) goes back to the suspended nanoparticles density (ρ_p) and their specific heat (c_p) respectively (as in Figure 2). So, the effective thermal conductivity (K_{eff}) of the spherical nanoparticle suspended nanofluids without considering interfacial layer with the combine effect of static and dynamic mechanisms ‘present model’ in Equation 11 can be simplified as Equation 12.

$$K_{eff} = \left\{ \frac{(K_p + 2K_f) + 2\varphi (K_p - K_f)}{(K_p + 2K_f) - \varphi (K_p - K_f)} \times K_f \right\} + \left\{ \frac{1}{2} \rho_p c_p d_s \sqrt{\frac{3K_B T(1-1.5\varphi)}{2\pi\rho_p r_p^3}} \right\} \quad (12)$$

The important features of this ‘present model’ (Equation 12) can be pointed out as bellow:

- (i) In the static and dynamic mechanism contributed model the effect of nanolayer is not considered.
- (ii) This model also able to estimate the temperature dependent thermal conductivity of a nanofluid.
- (iii) In Equation 12, the second part of the right-hand side is the dynamic mechanism contributed thermal conductivity (K_{dy}), which considers the effect of particles Brownian motion and temperature. The term, K_{dy} is appropriate for particles volumetric fraction of (φ) > 0.002 [26].
- (iv) If there is no interfacial layer considered, the static part of the developed model reduces back to the Maxwell model as in Equation 7. The dynamic part is (K_{dy}) renovated by replacing the nanoparticle parameters of complex particles terms using effective diffusion coefficient perception to integrate the effect of nanoparticles volumetric fraction on Brownian motion.

Results and Discussion

Structural and Particle Characterization

XRD Analysis

Figure 3 shows the acquired XRD pattern on the synthesized ironoxide particle sample. The diffractogram pattern shows well distinct peaks, this clearly indicates that the ironoxide sample is crystalline in form. No extra salt or ion is detected on XRD analysis. The diffraction peaks

at (2θ) 30.42, 35.60, 43.06, 53.40, 57.25 and 63.13⁰ are completely matched with the maghemite's ($\gamma\text{-Fe}_2\text{O}_3$) peaks. Square solid dots are placed to indicate the peak positions. The diffraction angles of these peaks are consistent with the standard from maghemite ($\gamma\text{-Fe}_2\text{O}_3$) (JCPDS No. 39-1346) [38]. It shows a reasonable match with previous results reported in the literature [10]. This confirms the formation of maghemite phase of ironoxide. The FWHM of the enlarged peak is used to estimate the average crystallite size with the aid of Scherrer's equation. The average crystallite size of the analyzed sample is found ~ 20.48 nm. The inter-planar spacing of maghemite sample is obtained about 2.51 which is same as the standard value of maghemite (2.51) compared with magnetite's (2.53) [39].

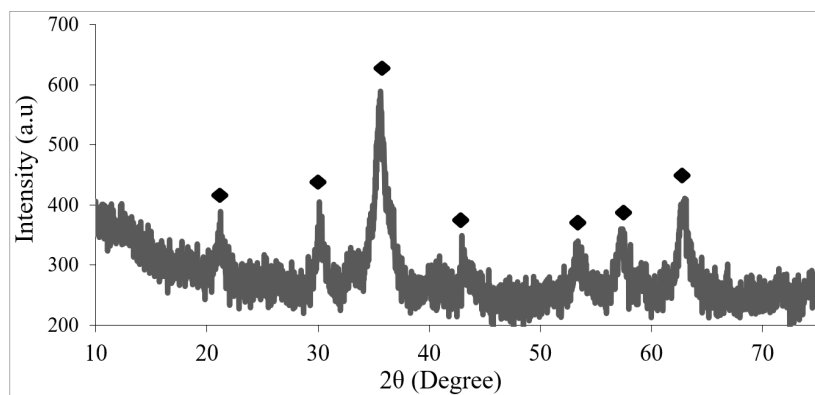


Figure 3 X-ray diffraction pattern of $\gamma\text{-Fe}_2\text{O}_3$ sample.

FESEM

FESEM image shows the morphology of the maghemite nanoparticles synthesised by chemical co-precipitation technique. Figure 4a displays the FESEM images of maghemite particles. It shows that the particles are mostly spherical in shape. Figure 4b shows the size distribution of the particles obtained from the FESEM analysis. For the estimation of average size of the synthesized MH nanoparticles, it was conducted the measurements of about 150 particles using image analysis software. It is found that, the sizes of the particles are varied from ~ 7.21 to ~ 80.45 nm among the measured particles. The data are summarized in the histogram in Figure 4b. It shows that, particles are uniformly distributed. The average size of the particle is obtained around 23.14 nm. Particle size roughly agrees with the data calculated from the XRD analysis.

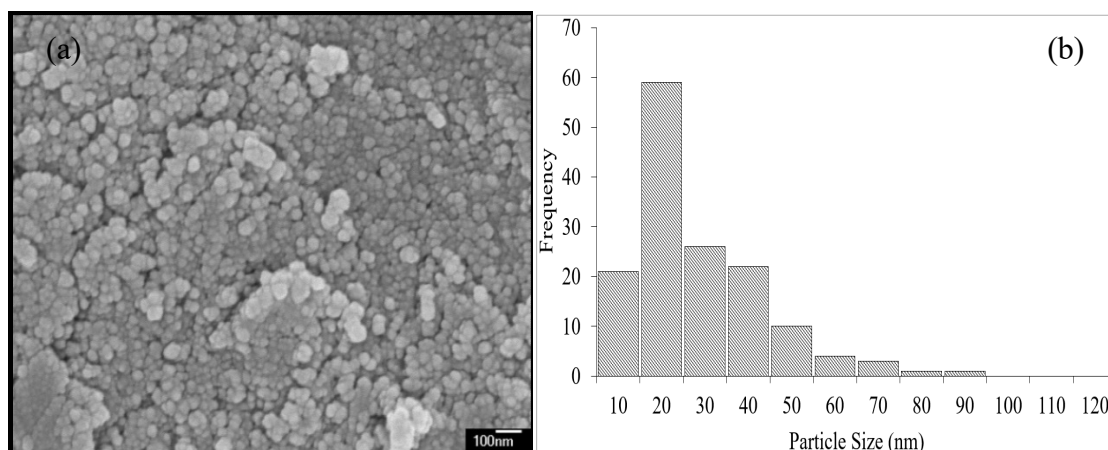


Figure 4 FESEM micrograph (a) and particle size distributions (b) of synthesized maghemite nanoparticles.

Thermogravimetric Analysis

Synthesised maghemite nanoparticle sample is maintained as highly purified by the careful washing process. The sample is filtered using the membrane filter of pore size $\leq 0.22 \mu\text{m}$ to achieve greater contact area and better equilibrium conditions. Thermogram in Figure 5 shows the weight loss phenomenon. It is seen that the weight loss occurs at about 100 °C. This weight loss occurs due to the evaporation of water from the sample [40]. Thermal gravimetric analysis is conducted on three separate samples of as produced MH nanoparticles. Each sample shows the almost similar weight loss characteristics.

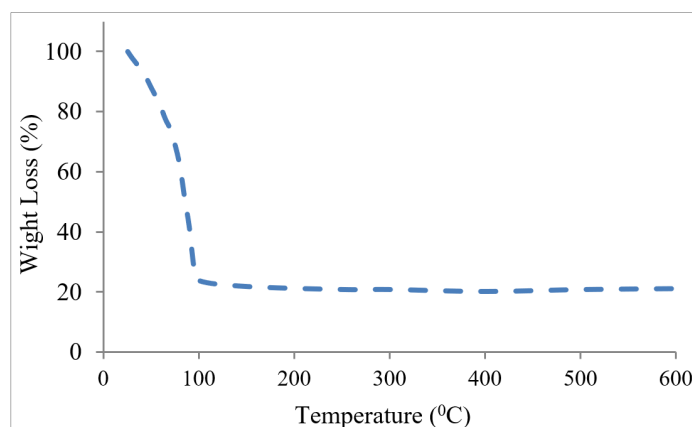


Figure 5 Thermogram of synthesized maghemite nanoparticle samples.

Magnetic Measurements

Prepared maghemite nanoparticles are dried and powder samples are characterized using external magnet to investigate their response to the magnetic field. Figure 6a shows the photographs of the magnetic illustration of the synthesized ironoxide nanoparticles using the

external magnetic field, induced by simple hand magnet. It shows that the powders are attracted to the bar magnet indicating that particles are magnetic. Figure 6b shows a typical hysteresis curve of the synthesized maghemite nanoparticles powder sample measured at 300K temperature using VSM. In this magnetization curve no hysteresis loop is evident. Meaning that both remanence magnetization and coercivity value is zero. It reveals that, the produced sample is superparamagnetic and particles are in nano-sized dimensions [19]. Saturation magnetization or maximum magnetization (M_{\max}) of the prepared maghemite sample is found to be 54.82 emu/g at an applied magnetic field of 10 kG. Obtained M_{\max} is also quite lower than the value for the bulk $\gamma\text{-Fe}_2\text{O}_3$ which is 85 emu/g [41]. It also leads to assume that the synthesized particles are maghemite ($\gamma\text{-Fe}_2\text{O}_3$).

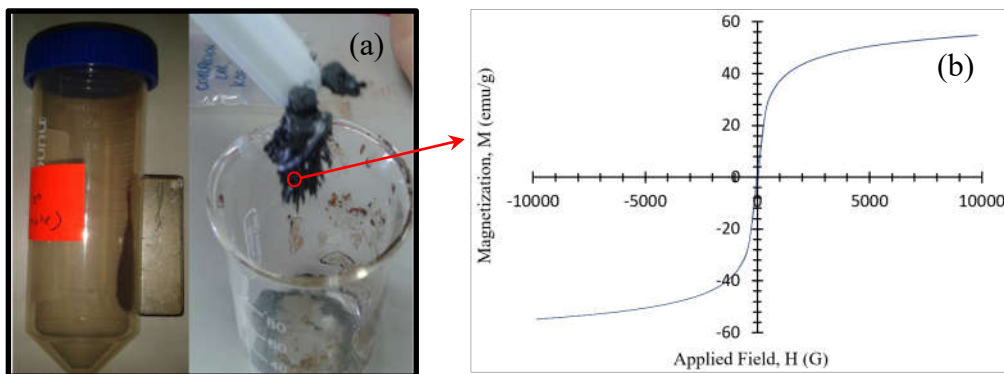


Figure 6(a) Illustrative photographs of magnetic nature of as produced maghemite nanoparticles interacting with the simple hand magnet; Figure 6(b) Hysteresis curve of maghemite ($\gamma\text{-Fe}_2\text{O}_3$) sample.

Physical Appearances of the MH/DW Nanofluids

Figure 7 shows the physical appearance in the digital photographs of MH/DW nanofluids. It displays very uniform distribution. Suspensions in the nanofluids are persisted very stable for nearly 3 to 4 months. Photographs of sample are captured after the preparation of 5 minutes then around 25 and 120 days. No visible sedimentation and agglomeration are shown with in the time investigated. Prepared MH/DW nanofluid shown very good stability against sedimentation explained elsewhere in the authors paper [42].

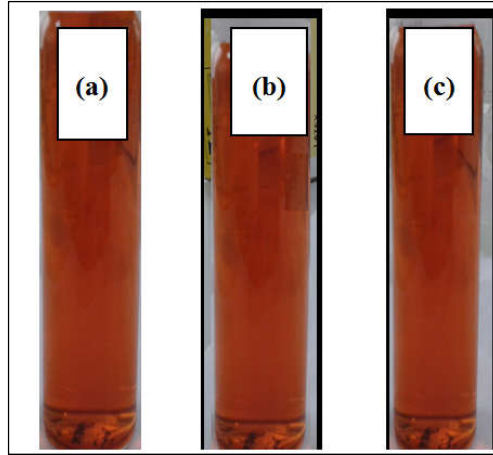


Figure 7: Physical appearances of MH/DW nanofluid: (a) after 5 minutes, (b) around 25 days and (c) around 120 days.

Percentage Thermal Conductivity Enhancements of MH/DW Nanofluids

Percentage thermal conductivity enhancements at different temperatures with the varying concentration of MH nanoparticles in DW is plotted in Figure 8. Percentage thermal conductivity enhancement is denoted as, $\eta = [(K_{nf} - K_f) / K_f] \times 100 \%$. Where, K_{nf} is the thermal conductivity of MH/DW nanofluids and K_f is the thermal conductivity of DW base fluid. In Figure 8 it is seen that, at room temperature sample S1-MH/DW obtained a marginal enhancement of thermal conductivity over the DW and this enhancement increased gradually with the increasing temperature which was about 10 % at 60 °C for this sample. Because the concentration of MH nanoparticles in DW is too low to increase the thermal conductivity and the low thermal conductivity of MH nanoparticles [43]. It reveals that the MH nanoparticle loading has an influence on the thermal conductivity enhancement of DW based nanofluids. It can be observed that, other samples of MH/DW nanofluids show higher enhancements of thermal conductivity at the higher temperature for the certain concentration of MH nanoparticles in DW. However, a bit higher rate of thermal conductivity enhancement is detected after 50 °C of temperature for all the MH/DW nanofluids.

The maximum enhancement of thermal conductivity is perceived for S5-MH/DW with the MH concentration of 0.157 mg/ml among the analysed samples. At 25 °C, it provides 4.5 % enhancements of thermal conductivity; then it reaches to about 32 % at a temperature of 60 °C. Because in this sample with higher concentration, the number of interactions among the particles is increased and the Brownian motion among the particles are raised at a higher temperature. Overall, it is detected that, thermal conductivities of MH/DW nanofluids are increased nonlinearly with the rise of temperature. With the rises of temperature, the frequency

of the of Brownian motion enhances remarkably, which results to the thermal conductivity enhancement equivalently. MH/DW nanofluids thermal conductivity goes higher with the increased concentration of MH nanoparticles than that of with the lower concentration due to the variations in Brownian motion intensity at higher temperature [25].

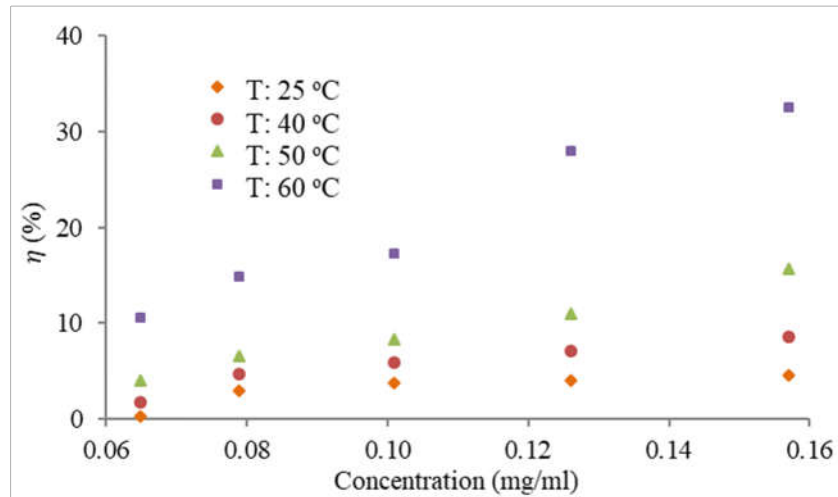


Figure 8 Percentage enhancement of thermal conductivity of the MH/DW nanofluid as a function of MH nanoparticle loading at temperature varies.

EFFECTIVE MEDIUM THEORIES FOR THERMAL CONDUCTIVITIES OF MH/DW NANOFLUIDS

Existing Models

The Maxwell model in Equation 7 is used as the illustrative of traditional models. Maxwell model was modified by Hasselman and Johnson (1987) [33] with the consideration of interfacial thermal resistance, R_{bd} (Equation 8 named as MG-EMA: HJ model). Figure 9 presents the relative (K_{nf}/K_f) enhancement of experimental thermal conductivity as a function of concentration of MH nanoparticles in base fluid DW. Effective thermal conductivity of MH/DW nanofluids samples is estimated by Maxwell model (Equation 7) where only thermal conductivity of MH/DW nanofluid (K_{nf}) and base fluid (K_f) and loading amount of MH nanoparticle in DW are considered. Besides, effective thermal conductivity of MH/DW nanofluids samples are also estimated by MG-EMA: HJ model, where thermal resistance, $R_{bd}=10^{-9} \text{ m}^2\text{K W}^{-1}$ is considered [44]. These predictions are also plotted in Figure 9 for the understanding of correlation of experiment with theory. It is seen that the experimental values of the K_{nf}/K_f are found to be increased with the increasing concentrations of MH nanoparticles in DW base fluid. However, the ratio K_{nf}/K_f is shown equal or slightly higher than 1 (one) for both the Maxwell model and MG-EMA: HJ prediction of MH/DW nanofluid samples. It means

that, predicted values of effective thermal conductivity of MH/DW nanofluid samples using Maxwell model and MG-EMA: HJ are like the thermal conductivity of base fluid DW.

It can be said that, Maxwell and MG-EMA: HJ model awfully under predict the MH/DW nanofluids thermal conductivity. It also reveals that, there is no interfacial thermal resistance is active with the MH nanoparticle and DW interface. Phenomenally, ratio K_{nf}/K_f for the sample S1-MH/DW shows somehow similar to the experiment and predictions. Reasonably enhancement of thermal conductivity of this sample is very marginal over DW base fluid. It might be the number of interactions among the particles is very less due to very low concentration. Estimated effective thermal conductivity by these models is not well agreed with the experimental thermal conductivity values of MH/DW samples. This recommends that, there is other mechanism contributed to the enhancements of thermal conductivity of MH/DW nanofluids.

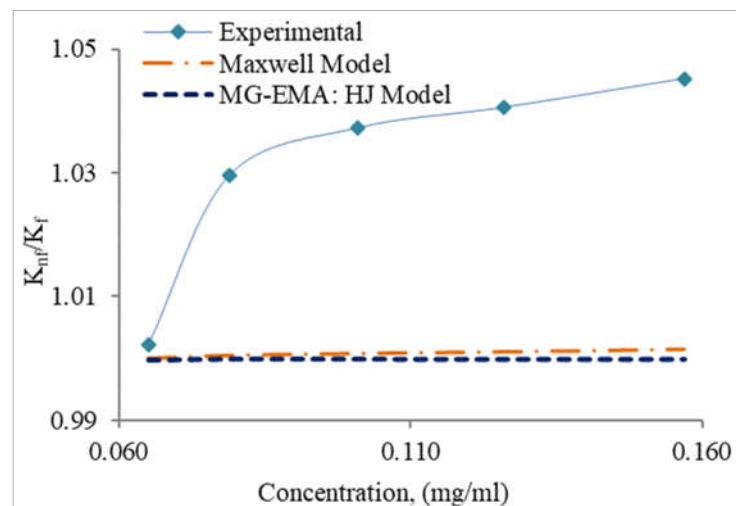


Figure 9 Relative thermal conductivity (K_{nf}/K_f) of MH/DW nanofluids as a function of concentration: Experimental with the Maxwell and MG-EMA: HJ model.

Combined Model for MH/DW Nanofluids

Figure 10 represents the experimental thermal conductivity of the MH/DW nanofluids samples with the varying temperature. Y-axis error bars with the experimental values are the errors in the thermal conductivity measurement of the MH/DW nanofluids. All errors with the experimental values are found to be ± 0.001 . Thermal conductivity of DW base fluid is also plotted with temperature for the comparison purpose. In Maxwell model, nanoparticles are considered static. In the modified model named 'present model' has been proposed for the spherical nanoparticle dispersion in the base fluid. In this model both static and dynamic contributions of nanoparticles are considered in thermal conductivity enhancement. In the

present model (Equation 12) no liquid layer was considered. So, static part of the present model falls back to the Maxwell model (Equation 7) and second part of the right-hand side of Equation 12 is the dynamic mechanisms contribution to the thermal conductivity, which considers the influence of particles Brownian motion and temperature. The term, K_{dy} in Equation 12 is not so suitable for the prediction of thermal conductivity with the particle volumetric fraction (ϕ) less than 0.002 [26]. Because of the inter-particle separation distance, d_s (Figure 2) is extremely wide to occur any contact by the Brownian force among the spherical nanoparticles [25, 37].

Predicted effective thermal conductivity by ‘present model’ of MH/DW nanofluid samples are plotted in Figure 10 with the experimental thermal conductivities. Figure 10(a) shows that the effective thermal conductivity of present model for sample S1-MH/DW over predicts from the experimental thermal conductivity. Volume fraction (ϕ) for S1-MH/DW was about 0.0013. For this reason, particles separation distance (d_s) is pretend to be very large in base fluid DW.

For the samples S2-MH/DW (0.079 mg/ml) and S3-MH/DW (0.101 mg/ml) ‘present model’ predicted closer than the S1-MH/DW (Figure 10(b-c)). Phenomenally, at some temperature it predicts slightly higher from the experimental values. In contrast, for the samples S4-MH/DW (0.126 mg/ml) and S5-MH/DW (0.157 mg/ml) in Figure 10(d-e) reveal that the ‘present model’ displays reasonably very good agreement with the experimentally measured results. It provides much better estimations with the comparison to Maxwell’s and MG-EMT: HJ models. It is because of the consideration of dynamic mechanism in MH nanoparticles during the rising temperature. With the rises of temperature, the frequency of Brownian motion enhances remarkably, which results to the enhancement of effective thermal conductivity equivalently for the MH/DW nanofluids. The frequency of the Brownian motion at higher temperature is instance in higher particle loading than that of in the lower loading of MH nanoparticle [25]. Thus, it reveals that for the single type of spherical particle dispersed nanofluids both static and dynamic mechanisms of the particles are considered to be involved for the enhancement of thermal conductivity of the nanofluids.

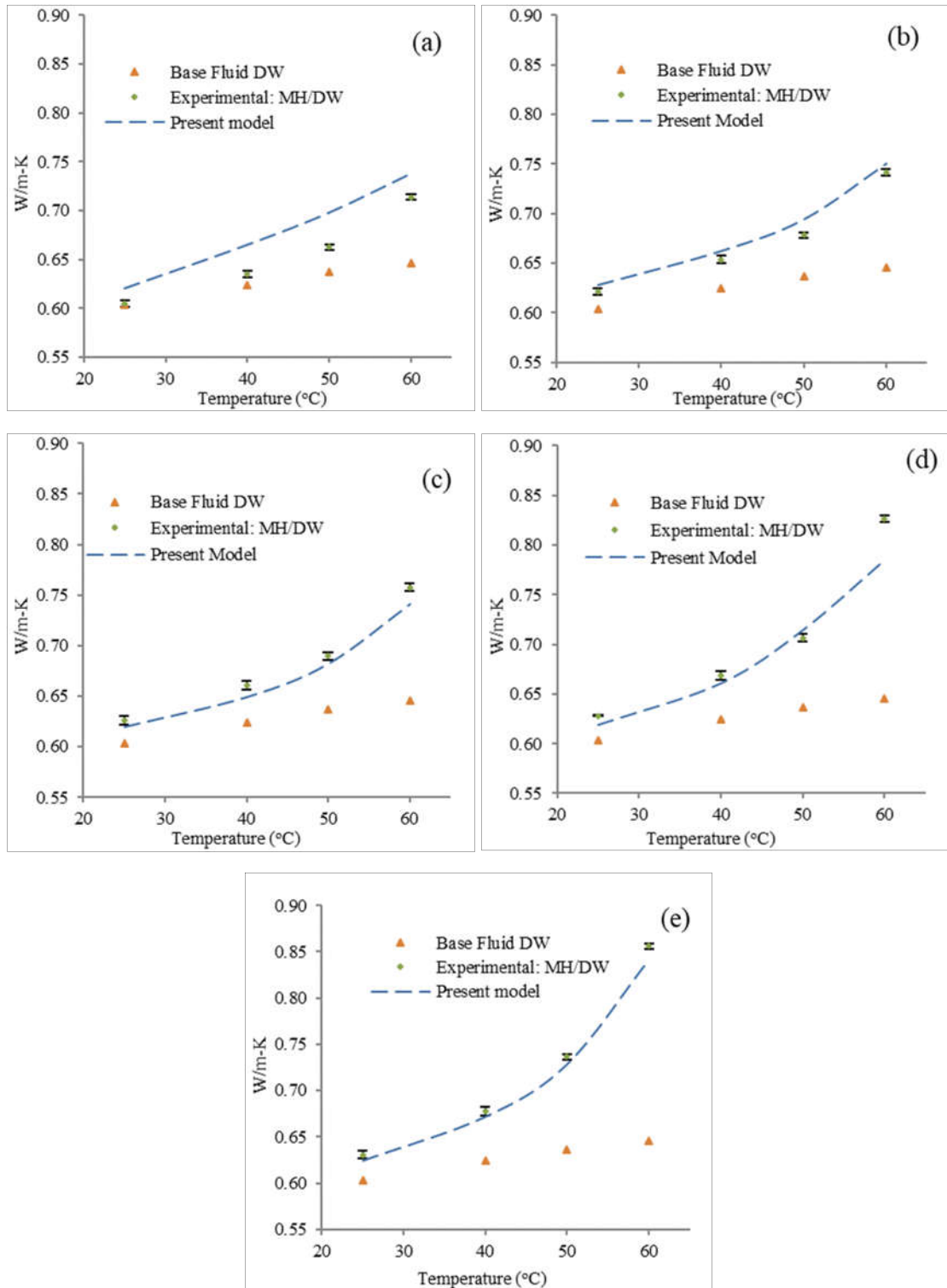


Figure 10: Thermal conductivity behaviour of MH/DW nanofluids with the increasing temperature and predictions by ‘present model’: (a) 0.065, (b) 0.079, (c) 0.101, (d) 0.126 and (e) 0.157 mg/ml.

Conclusions

Effective medium theories (EMTs) have been modified for the first time with the consideration of effects of static and dynamic mechanisms combinedly and evaluated the anomalous

behaviors of thermal conductivity enhancements of the spherical shaped maghemite nanoparticles dispersed nanofluids. In this purpose, maghemite nanoparticles of crystallite sizes around 20 nm were successfully synthesized by the wet chemical co-precipitation technique and characterized. Thermal conductivity of the prepared nanofluid samples were measured and analyzed with the varying MH nanoparticles loading and rising temperature. Investigation of thermal conductivity revealed that the enhancement of the thermal conductivity of MH/DW nanofluids increased linearly with the increasing MH nanoparticle concentration. However, enhancements of thermal conductivity of the MH/DW nanofluids were increased non-linearly with the increase in temperature. The maximum enhancement of thermal conductivity of MH/DW nanofluid was perceived with the MH concentration of 0.157 mg/ml among the analyzed samples. At 25 °C temperature, it provided 4.5 % enhancements of thermal conductivity over the DW base fluid and then it reached almost 32 % at 60 °C temperature. Prediction of effective thermal conductivity enhancements of produced MH/DW nanofluids by the Maxwell and MG-EMA: HJ model showed an awful under prediction from the experimentally measured thermal conductivities. Modified model with considering the static and dynamic mechanism of the MH nanoparticle showed reasonably very good agreement with the experimental thermal conductivities of MH/DW nanofluids at elevated temperature. This model is limited for the special nanoparticles, thus future works can be the insight analysis of the various other shapes of nanoparticles in the nanofluids for the various other thermophysical properties introducing possible different other parameters in this model farther.

Acknowledgements

The authors courteously acknowledge for allowing the lab facilities under Manufacturing and materials Engineering Department in International Islamic University Malaysia.

References

1. Bahiraei, M., et al., *Recent research contributions concerning use of nanofluids in heat exchangers: a critical review*. Applied Thermal Engineering, 2018. **133**: p. 137-159.
2. Agnihotri, P. and V. Lad, *Magnetic nanofluid: synthesis and characterization*. Chemical Papers, 2020: p. 1-12.
3. Khatai, S., et al., *Metal-oxide based nanofluid application in turning and grinding processes: A comprehensive review*. Materials Today: Proceedings, 2020.
4. Kumar, P.M., et al., *Review on nanofluids theoretical thermal conductivity models*. Engineering Journal, 2015. **19**(1): p. 67-83.

5. Liu, Y., et al., *Enhanced catalytic degradation of methylene blue by α -Fe₂O₃/graphene oxide via heterogeneous photo-Fenton reactions*. Applied Catalysis B: Environmental, 2017. **206**: p. 642-652.
6. Ghosh, S., et al., *Dimensional crossover of thermal transport in few-layer graphene*. Nature materials, 2010. **9**(7): p. 555-558.
7. Mehrali, M., et al., *Investigation of thermal conductivity and rheological properties of nanofluids containing graphene nanoplatelets*. Nanoscale research letters, 2014. **9**(1): p. 15.
8. Irwan, N., *Synthesis, characterization, and thermophysical properties of maghemite (γ -Fe₂O₃) nanofluids with and without magnetic fields effect*/Irwan Nurdin. 2016, University of Malaya.
9. Zenghu, H., *Nanofluids with Enhanced Thermal Transport Properties*. 2008, Ph. D. thesis, University of Maryland.
10. Darezereshki, E., *Synthesis of maghemite (γ -Fe₂O₃) nanoparticles by wet chemical method at room temperature*. Materials Letters, 2010. **64**(13): p. 1471-1472.
11. Wu, Z.-G. and J.-F. Gao, *Synthesis of γ -Fe₂O₃ nanoparticles by homogeneous coprecipitation method*. Micro & Nano Letters, 2012. **7**(6): p. 533-535.
12. Kleinstreuer, C. and Y. Feng, *Experimental and theoretical studies of nanofluid thermal conductivity enhancement: a review*. Nanoscale research letters, 2011. **6**(1): p. 229.
13. Sen Gupta, S., et al., *Thermal conductivity enhancement of nanofluids containing graphene nanosheets*. Journal of Applied Physics, 2011. **110**(8): p. 084302.
14. Choi, S., et al., *Anomalous thermal conductivity enhancement in nanotube suspensions*. Applied physics letters, 2001. **79**(14): p. 2252-2254.
15. Koblinski, P., et al., *Mechanisms of heat flow in suspensions of nano-sized particles (nanofluids)*. International journal of heat and mass transfer, 2002. **45**(4): p. 855-863.
16. Li, S.-Y., et al., *Effects of magnetic field on the pool boiling heat transfer of water-based α -Fe₂O₃ and γ -Fe₂O₃ nanofluids*. International Journal of Heat and Mass Transfer, 2019. **128**: p. 762-772.
17. Aich, D., et al., *Synthesis and Characterization of Super Paramagnetic Iron Oxide Nanoparticles*. Nanoscience & Nanotechnology-Asia, 2020. **10**(2): p. 123-126.
18. Racuciu, M., et al., *Room temperature synthesis of magnetic nanoparticles*. Journal of optoelectronics and advanced materials, 2008. **10**(11): p. 2928.
19. Tural, B., et al., *Preparation and characterization of surface modified γ -Fe₂O₃ (maghemite)-silica nanocomposites used for the purification of benzaldehyde lyase*. Journal of Physics and Chemistry of Solids, 2011. **72**(8): p. 968-973.
20. Hedayatnasab, Z., F. Abnisa, and W.M.A.W. Daud, *Review on magnetic nanoparticles for magnetic nanofluid hyperthermia application*. Materials & Design, 2017. **123**: p. 174-196.
21. Mohammadfam, Y., S.Z. Heris, and L. Khazini, *Experimental Investigation of Fe₃O₄/hydraulic oil magnetic nanofluids rheological properties and performance in the presence of magnetic field*. Tribology International, 2020. **142**: p. 105995.
22. Sarafraz, M., et al., *Pool boiling heat transfer characteristics of iron oxide nanosuspension under constant magnetic field*. International Journal of Thermal Sciences, 2020. **147**: p. 106131.
23. Karimi, A., et al., *Thermal Conductivity of Fe₂O₃ and Fe₃O₄ Magnetic Nanofluids Under the Influence of Magnetic Field*. International Journal of Thermophysics, 2015. **36**(10-11): p. 2720-2739.
24. Prasher, R., P. Bhattacharya, and P.E. Phelan, *Thermal conductivity of nanoscale colloidal solutions (nanofluids)*. Physical review letters, 2005. **94**(2): p. 025901.

25. Murshed, S., K. Leong, and C. Yang, *A combined model for the effective thermal conductivity of nanofluids*. Applied Thermal Engineering, 2009. **29**(11-12): p. 2477-2483.
26. Murshed, S.S., et al. *Contribution of Brownian motion in thermal conductivity of nanofluids*. in *Proceedings of the world congress on engineering*. 2011.
27. Yang, J., et al., *A combined theory model for predicting the viscosity of water-based Newtonian nanofluids containing spherical oxide nanoparticles*. Journal of Thermal Analysis and Calorimetry, 2019. **135**(2): p. 1311-1321.
28. Cui, W., et al., *Modified prediction model for thermal conductivity of spherical nanoparticle suspensions (nanofluids) by introducing static and dynamic mechanisms*. Industrial & Engineering Chemistry Research, 2014. **53**(46): p. 18071-18080.
29. Mohammadi, M., M. Dadvar, and B. Dabir, *Application of response surface methodology for optimization of the stability of asphaltene particles in crude oil by TiO₂/SiO₂ nanofluids under static and dynamic conditions*. Journal of Dispersion Science and Technology, 2018. **39**(3): p. 431-442.
30. Sundar, L.S., M.K. Singh, and A.C. Sousa, *Enhanced heat transfer and friction factor of MWCNT-Fe₃O₄/water hybrid nanofluids*. International Communications in Heat and Mass Transfer, 2014. **52**: p. 73-83.
31. Ramires, M.L., et al., *Standard reference data for the thermal conductivity of water*. Journal of Physical and Chemical Reference Data, 1995. **24**(3): p. 1377-1381.
32. Maxwell, J.C., *A treatise on electricity and magnetism*. Vol. 1. 1881: Clarendon press.
33. Hasselman, D. and L.F. Johnson, *Effective thermal conductivity of composites with interfacial thermal barrier resistance*. Journal of composite materials, 1987. **21**(6): p. 508-515.
34. Leong, K., C. Yang, and S. Murshed, *A model for the thermal conductivity of nanofluids—the effect of interfacial layer*. Journal of nanoparticle research, 2006. **8**(2): p. 245-254.
35. Bird, R., W. Stewart, and E. Lightfoot, *Shell energy balances and temperature distributions in solids and laminar flow*. Transport Phenomena. 2nd ed. John Willey and Sons, Inc., New York, NY, USA, 2002: p. 290-332.
36. Chandrasekhar, S., *Stochastic problems in physics and astronomy*. Reviews of modern physics, 1943. **15**(1): p. 1.
37. Jang, S.P. and S.U. Choi, *Role of Brownian motion in the enhanced thermal conductivity of nanofluids*. Applied physics letters, 2004. **84**(21): p. 4316-4318.
38. Nazari, M., et al., *Synthesis and characterization of maghemite nanopowders by chemical precipitation method*. Journal of Nanostructure in Chemistry, 2014. **4**(2): p. 99.
39. Tajabadi, M. and M. Khosroshahi, *Effect of alkaline media concentration and modification of temperature on magnetite synthesis method using FeSO₄/NH₄OH*. International Journal of Chemical Engineering and Applications, 2012. **3**(3): p. 206.
40. Chin, A.B. and I.I. Yaacob, *Synthesis and characterization of magnetic iron oxide nanoparticles via w/o microemulsion and Massart's procedure*. Journal of materials processing technology, 2007. **191**(1-3): p. 235-237.
41. Kilianová, M., et al., *Remarkable efficiency of ultrafine superparamagnetic iron (III) oxide nanoparticles toward arsenate removal from aqueous environment*. Chemosphere, 2013. **93**(11): p. 2690-2697.
42. A Arifuzzaman, A.F.I., Ahsan Ali Khan, M. Zahangir Alam and Saidur R, *Effect of Particle Loading on the Stability of the Water Based Iron-Oxide Nanofluids*. International Journal of Advanced Science and Technology 2020. **29** (1): p. 1326 - 1333.

43. Xie, H., et al., *Discussion on the thermal conductivity enhancement of nanofluids*. *Nanoscale research letters*, 2011. **6**(1): p. 124.
44. Baby, T.T. and R. Sundara, *Synthesis and transport properties of metal oxide decorated graphene dispersed nanofluids*. *The Journal of Physical Chemistry C*, 2011. **115**(17): p. 8527-8533.